BCL6 confers *KRAS*-mutant non–small-cell lung cancer resistance to BET inhibitors

Jiawei Guo,[1,2] Yanan Liu,[1] Jing Lv,[1] Bin Zou,[3] Zhi Chen,[1,4] Kun Li,[1] Juanjuan Feng,[1] Zhenyu Cai,[5] Lai Wei,[3] Mingyao Liu,[1] and Xiufeng Pang[1]

[1]Shanghai Key Laboratory of Regulatory Biology, Institute of Biomedical Sciences and School of Life Sciences, East China Normal University, Shanghai, China. [2]Department of Thoracic Surgery, State Key Laboratory of Biotherapy and Cancer Center, West China Hospital, Sichuan University and Collaborative Innovation Center for Biotherapy, Chengdu, China. [3]State Key Laboratory of Ophthalmology, Zhongshan Ophthalmic Center, Sun Yat-sen University, Guangzhou, China. [4]Medical Research Institute, Wuhan University, Wuhan, China. [5]Tongji University Cancer Center, Shanghai Tenth People's Hospital, School of Medicine, Tongji University, Shanghai, China.

The bromodomain and extra-terminal domain (BET) proteins are promising therapeutic targets to treat refractory solid tumors; however, inherent resistance remains a major challenge in the clinic. Recently, the emerging role of the oncoprotein B cell lymphoma 6 (BCL6) in tumorigenesis and stress response has been unveiled. Here, we demonstrate that BCL6 was upregulated upon BET inhibition in *KRAS*-mutant cancers, including non–small-cell lung cancer (NSCLC). We further found that BRD3, not BRD2 or BRD4, directly interacted with BCL6 and maintained the negative autoregulatory circuit of BCL6. Disrupting this negative autoregulation by BET inhibitors (BETi) resulted in a striking increase in BCL6 transcription, which further activated the mTOR signaling pathway through repression of the tumor suppressor death-associated protein kinase 2. Importantly, pharmacological inhibition of either BCL6 or mTOR improved the tumor response and enhanced the sensitivity of *KRAS*-mutant NSCLC to BETi in both in vitro and in vivo settings. Overall, our findings identify a mechanism of BRD3-mediated BCL6 autoregulation and further develop an effective combinatorial strategy to circumvent BETi resistance in *KRAS*-driven NSCLC.

Introduction

Cancer cells rely on "transcriptional addiction" to support their uncontrolled proliferation or other needs (1). This is largely attributed to the function of bromodomain and extra-terminal (BET) proteins (BRD2, BRD3, BRD4, and BRDT), which serve as epigenetic readers of lysine acetylation to activate gene transcription (2). Dysfunction of BET proteins has been strongly linked to the development and progression of various tumors (3). Specifically, BRD4 acts as a synthetic lethal factor of the proto-oncogene *MYC*, in which BRD4 not only promotes MYC transcription but also regulates its function and degradation (4, 5). Given the essential role of BET family proteins in cancer development and inflammation, more than 100 clinical trials are now being carried out to evaluate the benefits of BET inhibitors (BETi) as anticancer therapy (6). Although BETi show promising clinical benefits, inherent and acquired resistance is still inevitable. Furthermore, inherent BETi resistance often occurs because of increased BET protein stability, which is triggered either by a weakened ubiquitination of *SPOP*-mutant status (7) or enhanced deubiquitination in a DUB3-dependent manner (8). In contrast, acquired BETi resistance is largely attributed to the reactivation of MYC expression, which is partly a consequence of

increased Wnt/β-catenin signaling (9) or the formation of a BRD4-MED1 transcription complex (10). Therefore, it is paramount to further elucidate the mechanism underlying BETi resistance and explore the potential treatment paradigms to sensitize the cancer response to BET inhibition in a specific tumor context.

B cell lymphoma 6 (BCL6) is a member of the BTB/POZ-zinc finger family of transcription factors and mediates transrepression (11). As a proto-oncogene in diffuse large B cell lymphoma, BCL6 drives the malignant phenotype by regulating hundreds of target genes involved in cell proliferation (12), DNA damage sensing (13), senescence (14), and antiapoptosis (15). BCL6 has been implicated in the promotion of an expanding scope of hematologic and solid tumor progression (16, 17), including that of non–small-cell lung cancer (NSCLC) (18). Compounds selectively targeting BCL6 activity have demonstrated promising antitumor effects in preclinical settings (19, 20). Recent work has shown that BCL6 serves as a central component of the stress response and tumorigenesis, in which inhibition of BCL6 might potentiate chemotherapeutic sensitivity (21, 22). These findings highlighted a key role of BCL6 in conferring cancer cell resistance to therapeutic agents.

KRAS-mutant NSCLC represents an enormous health burden because of its high motility. A series of clinical trials are now being carried out to explore potential therapeutic options (23). Although our previous studies have unveiled vulnerability of *KRAS*-mutant cancers that can be tractable with the use of either monotherapy (24) or a combined regimen (25), *KRAS*-mutant NSCLC remains refractory to all targeted therapies to date (26). Given the critical role of BCL6 in mediating stress tolerance, we hypothesize that
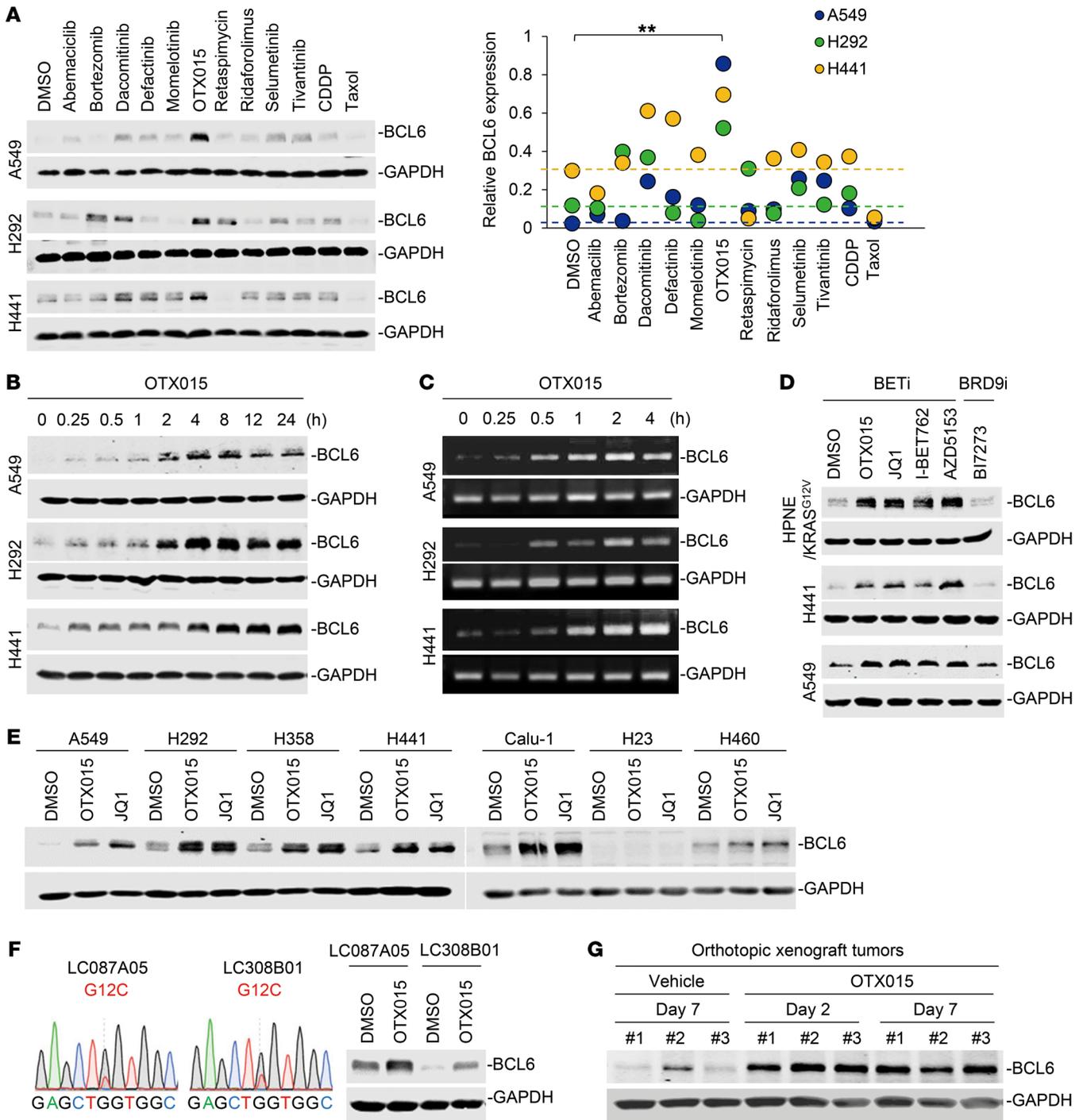
JCI

Figure 1. Clinical BETi promote BCL6 expression. (**A**) BCL6 expression in *KRAS*-mutant NSCLC cells in response to clinical drug treatments. Cells were treated with the indicated drugs at a concentration of their one-half IC$_{50s}$ for 48 hours. Graph shows the relative BCL6 protein levels, normalized to GAPDH. **P < 0.01, by unpaired, 2-tailed Student's *t* test, comparing the relative BCL6 protein level of the OTX015-treated group with that of the vehicle-treated group. (**B** and **C**) OTX015 upregulated BCL6 expression at the (**B**) protein and (**C**) transcription levels in a time-dependent manner. A549, H292, and H441 cells were treated with OTX015 for the indicated durations. BCL6 expression was detected by Western blotting and PCR assays. (**D**) BCL6 protein levels in cells upon treatment with BETi (OTX015, JQ1, I-BET762, and AZD5153) or a BRD9i (BI7273). (**E**) BETi upregulated BCL6 expression in a set of *KRAS*-mutant NSCLC cells. Cells were treated with OTX015 (300 nM), JQ1 (300 nM), or DMSO for 6 hours. Cell lysates were probed with antibodies against BCL6 and GAPDH. (**F**) OTX015 upregulated BCL6 levels in 2 primary NSCLC cell lines harboring a *KRAS*^{G12C} mutation. Left: DNA-Seq of exon 2 in the *KRAS* gene. Right: BCL6 levels in LC087A05 and LC308B01 cells exposed to OTX015 (300 nM) or DMSO for 6 hours. (**G**) BCL6 protein levels in orthotopic xenografts. During the 1-week treatment with OTX015, tumor tissue was isolated on day 2 and day 7, followed by immunoblot analysis for BCL6 expression. Three biologically independent samples per group are shown.

BCL6 may confer resistance to targeted therapies in *KRAS*-mutant NSCLC. To this end, we tested a set of clinical drugs that are either approved or under clinical evaluation to treat *KRAS*-mutant NSCLC. Intriguingly, we found that BCL6 was upregulated upon BET inhibition. We further observed that BRD3, not BRD2 or BRD4, directly interacted with BCL6, functioning as a BCL6 partner to maintain the negative autoregulatory circuit of BCL6. Upon BET inhibition, the transrepression of BCL6 was disrupted and consequently activated the mTOR signaling pathway to tolerate BET inhibition. These findings further support an effective combinatorial strategy with potential translatability to sensitize *KRAS*-mutant NSCLC to clinical BETi by concurrent inhibition of either BCL6 or mTOR.

Results

Clinical BETi promote BCL6 transcription. Given the critical role of BCL6 in tumorigenesis and the stress response, we hypothesized that BCL6 might confer resistance to targeted therapies in *KRAS*-mutant NSCLC. To this end, we tested a set of clinical drugs (Supplemental Table 1; supplemental material available online with this article; https://doi.org/10.1172/JCI133090DS1) that have either been approved or are currently under clinical evaluation to treat *KRAS*-mutant NSCLC to determine their impact on the protein expression of BCL6. Intriguingly, we found that OTX015, a clinical BETi, induced a striking and significant increase in BCL6 protein levels across 3 different *KRAS*-mutant NSCLC cell lines (Figure 1A), implying a potential role of BCL6 in the BETi response. Specifically, OTX015 time dependently induced a rapid increase in BCL6 protein levels at the tested dose (Figure 1B), without affecting cancer cell viability (Supplemental Figure 1A). These data excluded an indirect effect of cell death, selecting for BCL6hi cells by OTX015 treatment. Subsequently, we determined that OTX015-mediated BCL6 upregulation was due to an increase in BCL6 gene expression (Figure 1C and Supplemental Figure 1B) rather than a decrease in protein degradation (Supplemental Figure 1, C and D). These data collectively indicate that OTX015-induced BCL6 upregulation occurred at the transcription level at early time points, before cytotoxicity was observed.

In an attempt to exclude an off-target effect of OTX015, we used 3 other BETi (JQ1, I-BET762, and AZD5153) and 1 BRD9 inhibitor (BRD9i) (BI7273) in the experimental system. As expected, HPNE/KRASG12V (a normal pancreatic epithelial cell line with an introduced *KRAS*G12V variant), H441, and A549 cells strikingly upregulated BCL6 protein levels in response to 4 different BETi, but they failed to respond to BI7273 (Figure 1D), suggesting the specificity of BET inhibition in promoting BCL6 expression.

Of note, we also observed increased BCL6 expression provoked by BETi in a panel of *KRAS*-mutant lung (Figure 1E), colorectal, and pancreatic cancer cell lines (Supplemental Figure 2A and Supplemental Table 2), and in 2 primary *KRAS*-mutant NSCLC cell lines (LC087A05 and LC308B01) harboring a *KRAS*G12C mutation (Figure 1F). In total, 12 of 15 *KRAS*-mutant cancer cell lines showed increased BCL6 expression, thus reinforcing a general action of BETi in this specific tumor context.

BCL6 functions as a key transcriptional repressor by recruiting cofactors to suppress target genes (11). Our results further showed that the increased BCL6 induced by OTX015 accumu-

lated in nuclei (Supplemental Figure 2B) and repressed several well-known BCL6 target genes, such as *CASP8*, *CDKN1A*, *CHEK1*, *DUSP5*, and *TP53* (Supplemental Figure 2C). These data reveal that increased expression of BCL6 triggered by BET inhibition has functionality in cells.

Inhibitors of the BET family of proteins have shown promising anticancer activity in multiple myeloma, leukemia, and prostate cancers (27–29). However, BETi have been reported to be less effective in *KRAS*-mutant NSCLC (30). In agreement with our assumption that BCL6 induction contributes to BETi failure, we found that BCL6 expression was increased in orthotopic xenograft tumors isolated from tumor-bearing mice treated with 50 mg/kg/d OTX015 over a period of 1 week (Figure 1G). These results collectively support the notion that BET inhibition increases BCL6 expression in *KRAS*-mutant NSCLC in vitro and in vivo.

BCL6 is required for the therapeutic efficacy of BET inhibition. In attempting to clarify the role of increased BCL6 expression in the therapeutic efficacy of clinical BETi, we overexpressed BCL6 in two *KRAS*-mutant A549 and H23 cell lines and subsequently treated these cells with various concentrations of OTX015. Our results showed that BCL6 overexpression significantly increased the IC$_{50}$ of OTX015 by more than 5-fold in A549 cells (Figure 2, A and B). The phenomenon of BCL6-mediated BETi resistance was additionally confirmed by colony formation assays, in which the inhibitory effects of OTX015 on A549 cell viability were markedly decreased by BCL6 overexpression (Figure 2C). We obtained consistent results in H23 cells (Figure 2, D–F).

Next, we investigated whether direct BCL6 silencing could, in turn, sensitize cancer cells to BET inhibition. Therefore, we genetically interfered with BCL6 expression in BCL6hi H441 cells and evaluated the effects of BCL6 knockdown on OTX015 sensitivity by colony formation assays. As expected, both siRNAs targeting BCL6 potentiated OTX015 cytotoxicity and efficacy (Figure 2G). On the basis of these observations, we further applied different concentrations of BI3802, a recently developed BCL6 degrader (20), along with OTX015, and examined the antigrowth effects of various drug combinations on *KRAS*-mutant A549 cells. Our results showed that BCL6 degradation effectively sensitized OTX015 (Figure 2H). Collectively, these results establish that BCL6 plays a substantial role in conferring BETi resistance.

BET inhibition disrupts the BCL6 autoregulatory circuit. Considering that BCL6 upregulation was caused by increased BCL6 transcription rather than decreased protein degradation (Figure 1C and Supplemental Figure 1, B–D), we sought to explore the mechanism underlying the increased transcription of BCL6. It has been reported that BCL6 binds to its promoter to repress its own transcription (16, 31), therefore, we asked whether BET inhibition caused disruption of this negative autoregulatory circuit of BCL6, and consequently promoting its expression. To this end, we performed ChIP with massively parallel DNA-Seq (ChIP-Seq) using a BCL6 antibody and observed a complete shift of BCL6 binding from its promoter regions (region 1 and region 2) to its coding regions (region 3) (Figure 3A). This finding was additionally confirmed by ChIP-quantitative PCR (ChIP-qPCR) analysis (Figure 3B). Such a shift was of biological function, as the binding of RNA polymerase II (Pol II) was dramatically increased while dissociating BCL6 from its promoter regions (region 1 and region
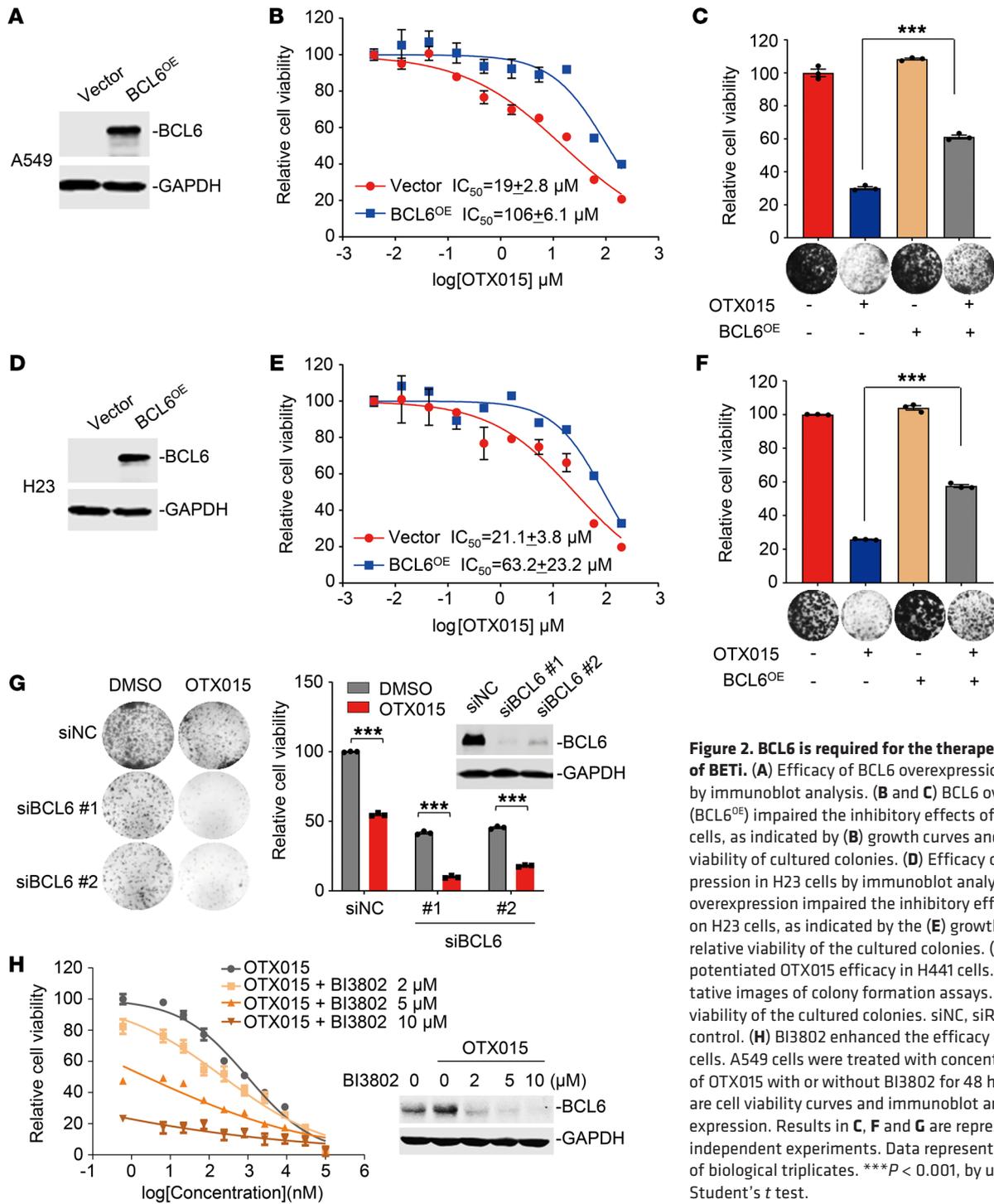
Figure 2. BCL6 is required for the therapeutic efficacy of BETi. (**A**) Efficacy of BCL6 overexpression in A549 cells by immunoblot analysis. (**B** and **C**) BCL6 overexpression (BCL6^{OE}) impaired the inhibitory effects of OTX015 on A549 cells, as indicated by (**B**) growth curves and (**C**) relative cell viability of cultured colonies. (**D**) Efficacy of BCL6 overexpression in H23 cells by immunoblot analysis. (**E** and **F**) BCL6 overexpression impaired the inhibitory effects of OTX015 on H23 cells, as indicated by the (**E**) growth curves and (**F**) relative viability of the cultured colonies. (**G**) BCL6 silencing potentiated OTX015 efficacy in H441 cells. Left: Representative images of colony formation assays. Right: Relative viability of the cultured colonies. siNC, siRNA negative control. (**H**) BI3802 enhanced the efficacy of OTX015 in A549 cells. A549 cells were treated with concentration gradients of OTX015 with or without BI3802 for 48 hours. Shown are cell viability curves and immunoblot analysis of BCL6 expression. Results in **C**, **F** and **G** are representative of 3 independent experiments. Data represent the mean ± SEM of biological triplicates. ***$P < 0.001$, by unpaired, 2-tailed Student's *t* test.

2) (Figure 3C), suggesting that the autoregulatory circuit of BCL6 was apparently disrupted upon BET inhibition. In contrast, we observed no obvious binding of RNA Pol II in the *BCL6* coding region (region 3; Figure 3C).

To further understand the biological role of BCL6 promoter regions, we cloned region 1 and region 2 to generate luciferase reporter vectors (named P1-Fluc and P2-Fluc). These vectors, along with an empty vector (named P0-Fluc), were respectively transfected into A549 cells. Our results showed that OTX015 significantly increased reporter gene expression of P1-Fluc and

P2-Fluc (Figure 3D). The phenomenon that region 2 exhibited much higher baseline signal than did region 1 might be attributed to differential enrichment of RNA Pol II binding, as shown in Figure 3C. We next investigated the impact of BCL6 on these promoter regions by further genetically silencing BCL6 in those experimental cells. Our results showed that BCL6 knockdown significantly increased reporter gene expression (Figure 3E). Collectively, these results establish a mechanism whereby BET inhibition causes disruption of the BCL6 autoregulatory circuit and provokes BCL6 transcription.
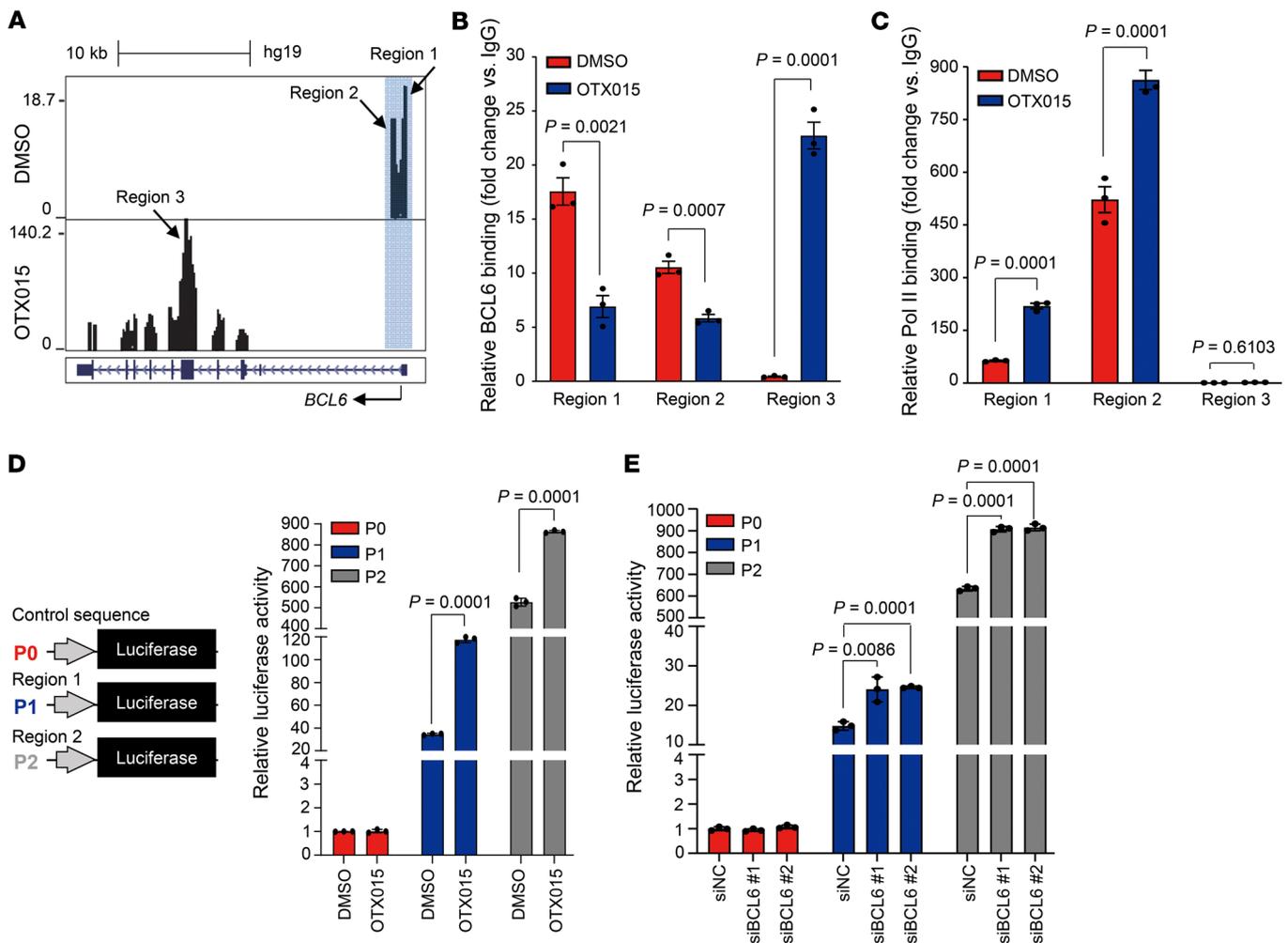
Figure 3. BET inhibition disrupts the BCL6 autoregulatory circuit. (**A**) OTX015 treatment shifted BCL6 from binding its promoter regions (region 1 and region 2) to its coding region (region 3). A549 cells were treated with DMSO or OTX015 (300 nM) for 6 hours. Chromatin was sheared and subsequently precipitated using a specific antibody against BCL6. Cellular DNA for the ChIP assay was isolated and analyzed on an Illumina NextSeq 500 instrument. Reads were mapped to the human reference genome (GRCh37/hg19) using Bowtie2 (version 2.2.9). UCSC's Genome Browser tracks showed BCL6 ChIP-Seq signals in the *BCL6* gene locus. Blue shading marks the peaks located in the promoter region. (**B**) OTX015 treatment promoted BCL6 to bind to its coding region. qPCR was performed with primers specifically targeting region 1, region 2, and region 3 of the *BCL6* gene. The data are plotted relative to the values obtained with the IgG control antibody. Data represent the mean ± SEM of biological triplicates. *P* values were analyzed by unpaired, 2-tailed Student's *t* test, comparing the OTX015 treatment group with the control group. (**C**) RNA Pol II–binding level at the 3 indicated regions examined by ChIP-qPCR. Data represent the mean ± SEM of biological triplicates. *P* values were determined by unpaired, 2-tailed Student's *t* test, comparing the OTX015 treatment group with the control group. (**D**) Response of different BCL6 promoter (P) regions to OTX015 treatment. Luciferase reporter vectors with promoters containing the indicated BCL6 promoter regions (region 1 and region 2) or the control sequence were equivalently transfected into A549 cells. Transfected cells were then exposed to 300 nM OTX015. Cells were harvested to detect luciferase expression 48 hours after transfection. Data represent the mean ± SD of biological triplicates. *P* values were determined by unpaired, 2-tailed Student's *t* test, comparing the OTX015 treatment group with the control group. (**E**) Response of different BCL6 promoter regions to BCL6 silencing. Luciferase reporter vectors with promoters containing the indicated BCL6 promoter regions (mentioned in **D**) or the control sequence were equivalently transfected into BCL6-knockdown A549 cells. Transfected cells were harvested to detect luciferase expression 48 hours after transfection. Data represent the mean ± SD of biological triplicates. *P* values were determined by unpaired, 2-tailed Student's *t* test, comparing the siBCL6 groups with the control group.

BRD3 acts as a cofactor to maintain the BCL6 autoregulation circuit. Given that current BETi, such as OTX015 and JQ1, are unable to distinguish between BRD2, BRD3, and BRD4, we carried out a knockdown assay to determine which BET protein contributed to BCL6 upregulation. Intriguingly, we found that genetic silencing of BRD2 and BRD3, rather than BRD4, markedly increased BCL6 expression in *KRAS*-mutant A549 (Figure 4A) and H441 cells (Supplemental Figure 3A), implying that BRD2 and BRD3 participated in BCL6 regulation in unstressed conditions. These findings

were further supported by the failure of the BRD4-specific inhibitors DC-1 and DC-2 (32) to promote BCL6 expression (Figure 4B), even at higher concentrations (Supplemental Figure 3B). On the basis of the above results, we speculated that these BET family proteins might directly interact with BCL6 protein. To this end, we performed an immunoprecipitation assay and found that only BRD3 directly bound to BCL6, whereas no obvious interaction was detected between BCL6 and BRD2 or BRD4 in A549 cells (Figure 4C). We observed similar results in H441 cells (Supplemental
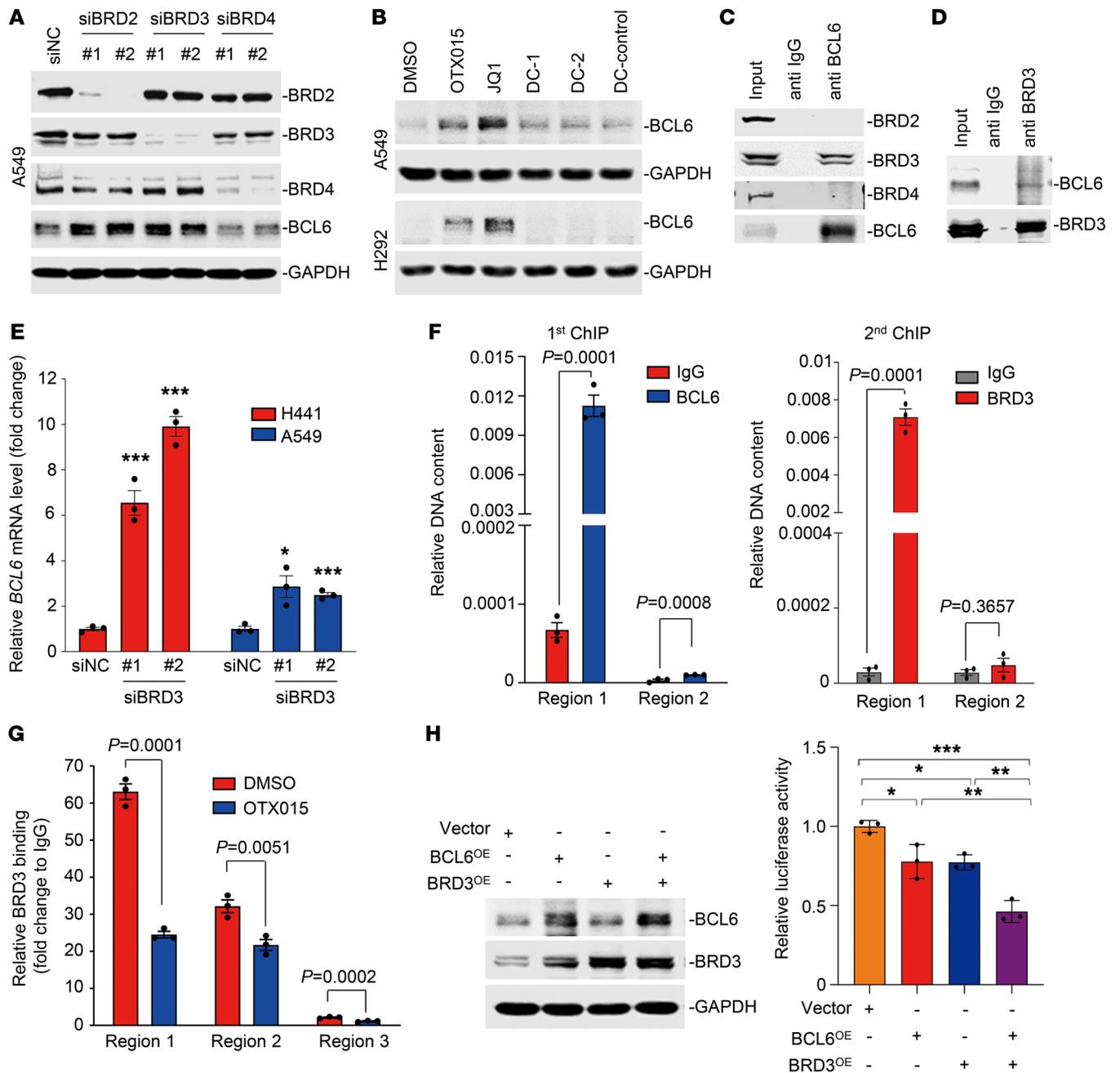
Figure 4. BRD3 acts as a cofactor to maintain BCL6 autoregulation. (**A**) Knockdown of BRD2 or BRD3 upregulated BCL6 expression. A549 cells transfected with 20 nM siRNAs targeting BRDs were collected 48 hours after transfection. BRD2, BRD3, BRD4, and BCL6 expression were detected by immunoblot analysis. (**B**) BRD4-specific inhibitors did not affect BCL6 expression. A549 and H292 cells were treated with BETi (OTX015 and JQ1), BRD4-specific inhibitors (DC-1 and DC-2), or a negative control compound (DC-control) for 6 hours. (**C** and **D**) Endogenous interaction of BCL6 and BRD3. A549 cell lysates were subjected to immunoprecipitation experiments using an anti-BCL6 or anti-BRD3 antibody. Immunoprecipitates were analyzed with antibodies against BRD2, BRD3, BRD4, and BCL6. Ten percent of total lysates was used as the input control. The anti-IgG antibody was used as a negative control. (**E**) Knockdown of BRD3 increased BCL6 mRNA levels. Data represent the mean ± SEM of biological triplicates. *P* values were analyzed by comparing siBRD3 groups with the control group. *P < 0.05 and ***P < 0.001, by unpaired, 2-tailed Student's *t* test. (**F**) ChIP and re-ChIP were performed to test the cobinding of the BCL6 and BRD3 complex at the loci on the BCL6 promoter regions mentioned in Figure 3A. The first ChIP was performed using anti-BCL6 and anti-IgG antibodies. The second ChIP was performed using anti-BRD3 and anti-IgG antibodies to analyze the first ChIP (anti-BCL6) components. Data represent the mean ± SEM of biological triplicates. *P* values were analyzed by Student's *t* test analysis for the first and second ChIPs. (**G**) BRD3 binding at the 3 indicated regions analyzed by ChIP-qPCR. Data represent the mean ± SEM of 3 independent experiments. *P* values were determined by unpaired, 2-tailed Student's *t* test. (**H**) BRD3 maintained the BCL6 autoregulatory circuit. A549 cells were cotransfected with P1-Fluc, together with an equivalent amount of pcDNA3.1-BRD3, pcDNA3.1-BCL6, and/or pcDNA3.1-Ctrl. Cells were harvested for a luciferase assay 48 hours after transfection. Western blotting was subsequently conducted using specific antibodies against BCL6, BRD3, and GAPDH. Data represent the mean ± SD of biological triplicates. *P < 0.05, **P < 0.01, and ***P < 0.001, by 1-way ANOVA. Immunoblots in **A**, **C**, and **D** were contemporaneous and run in parallel from the same biological replicate.

Figure 3C), excluding a cell-line–specific effect. We further confirmed the endogenous interaction between BRD3 and BCL6 by a reverse immunoprecipitation analysis of A549 cells (Figure 4D).

To understand the mechanism of BRD3 in regulating BCL6, we genetically interfered with BRD3 and found a marked increase in BCL6 transcription (Figure 4E). Given the endogenous interaction between BRD3 and BCL6, we thus hypothesized that the BRD3-BCL6 complex might bind to the BCL6 functional promoter regions (region 1 and region 2). A sequential ChIP (ChIP/re-ChIP) assay was further carried out to investigate their binding patterns. The immunoprecipitation by anti-BCL6 antibody served as the first ChIP component, which was then subjected to a second ChIP assay using a specific antibody against BRD3. The results revealed a marked co-occupancy of BRD3 and BCL6 on BCL6 promoter region 1, rather than region 2 (Figure 4F), indicating that BRD3 and BCL6 exist in the same protein complex that preferentially binds to the promoter region 1 of the *BCL6* gene in unstressed conditions. As expected, addition of OTX015 attenuated the interaction of BRD3 and BCL6 (Supplemental Figure 3D) and further impaired the binding of BRD3 to BCL6 promoter region 1, as region 1 binding exhibited a more rapid decrease upon OTX015 treatment (Figure 4G). In light of these data, we next examined whether the interaction between BRD3 and BCL6 contributes to BCL6 negative autoregulation. Using the P1-Fluc luciferase reporter assay, we found that BRD3 overexpression significantly enhanced BCL6 autorepression (Figure 4H and Supplemental Figure 3E), highlighting a cooperativity of BRD3 and BCL6 to maintain the BCL6 autoregulatory circuit.

Given that BRD3 acted as a regulator of BCL6, we asked whether they coordinated to regulate gene transcription in a more general pattern. Through a random examination of sequencing tracks along human chromosome 12, we found obvious colocalization of BCL6 with BRD3 peaks at the genome-wide level (Supplemental Figure 4A). Moreover, we compared BCL6- and BRD3-binding peaks and found that they potentially shared a great number of binding sites, nearly half of which (promoter 12% plus exon 6% plus intron 29%) were located in gene bodies (Supplemental Figure 4B). Since BCL6 functions as a transcriptional repressor, we thus elucidated the working mechanism of BCL6 and BRD3 cooperatives by analyzing gene promoters. Our data showed that among the 694 BCL6-binding gene promoters, 82 genes (2.6%) also harbored BRD3 binding (Supplemental Figure 4C and Supplemental Table 3). Additionally, the core element in the BCL6-binding consensus sequence was nearly identical to the BRD3-binding motif, which presented a typical palindrome (Supplemental Figure 4D). More specifically, we detected strong colocalization of BRD3 and BCL6 in the promoter regions of *CPD*, *IDH2*, *IRT1* and of *BCL6* itself (Supplemental Figure 4E), which was further confirmed by ChIP-qPCR experiments (Supplemental Figure 4F and Figure 4F). Together, these findings reveal that BRD3 works, in part, as a BCL6 partner and coordinately regulates shared gene expression.

Increased BCL6 expression activates mTOR signaling through suppression of DAPK2. After elucidating the regulatory effects of BETi on BCL6, we next sought to characterize BCL6 downstream components to decipher its detailed role in *KRAS*-mutant NSCLC. BET inhibition produced a BCL6 gene–binding spectrum that was quite different from that of the vehicle-treated cells. BCL6 bound

to the promoter region of 577 genes upon vehicle treatment and of 614 genes upon OTX015 treatment, with only 117 (8.9%) overlapping genes (Figure 5A and Supplemental Table 4). These results may be explained by the aforementioned BET-dependent mechanism, whereby BRD3 cooperated with BCL6 to regulate the latter's target genes.

Because BCL6 is a well-known transcriptional repressor, we therefore performed an RNA-Seq assay to identify genes whose transcription was affected by OTX015 treatment. We compared the 614 BCL6-binding genes unique to OTX015 treatment with our RNA-Seq data. As listed in Figure 5B, transcription of 51 BCL6-binding genes was significantly changed by OTX015 treatment ($P < 0.05$). Of the 32 significantly downregulated genes, death-associated protein kinase 2 (*DAPK2*) was the only putative tumor suppressor whose downregulation was strongly associated with enhanced tumor cell survival (33, 34). Our ChIP-Seq data revealed increased binding of BCL6 to the promoter of *DAPK2* upon OTX015 treatment (Figure 5C), which we additionally confirmed by ChIP-qPCR (Figure 5D). Of note, the binding of BCL6 repressed *DAPK2* transcription, as RNA Pol II enrichment was significantly decreased upon treatment with OTX015 (Figure 5E). Consistently, OTX015 treatment decreased *DAPK2* mRNA levels in different *KRAS*-mutant NSCLC cell lines (Figure 5F), underlining a more general phenotype of *DAPK2* transrepression by BET inhibition. DAPK2 has been reported to suppress mTOR signaling (35). In agreement, we found that OTX015 negatively regulated DAPK2 expression and positively activated mTOR signaling in a time-dependent manner in *KRAS*-mutant A549 cells, resulting in specific effects on P70S6K and 4E-BP1, two regulatory components downstream of the mTOR kinase (Figure 5G). We observed similar results in H292 and H441 cells (Figure 5H). Importantly, the decrease in DAPK2 expression and the increase in mTOR activity by OTX015 were dramatically diminished by BCL6 knockdown (Figure 5I), suggesting that DAPK2/mTOR signaling is dependent on the regulation of BCL6 in treated cells.

BCL6 inhibitors synergize with BETi in vitro and in vivo. Given that BCL6-mediated mTOR signaling is activated upon BET inhibition, we sought to test whether current BCL6-specific inhibitors, such as FX1 (19) and Compound 7 (36), are capable of sensitizing *KRAS*-mutant NSCLC cells to BET inhibition. To this aim, we combined BCL6 inhibitors (FX1 and Compound 7) with BETi (OTX015, JQ1, and I-BET762) to examine their synergistic effects. To indicate drug interactions, we calculated the combination indices (CIs) at 50%, 75%, and 90% of the effective dose (ED_{50}, ED_{75}, and ED_{90}) of each drug pair. Our results showed that concurrent inhibition of BCL6 and BET produced strong synergy (CI <0.7) in 5 different *KRAS*-mutant NSCLC cell lines (Figure 6A). Cotreatment with FX1 and OTX015 inhibited the colony formation ability of *KRAS*-mutant cells (Figure 6B and Supplemental Figure 5, A and B) and primary *KRAS*-mutant NSCLC cells (LC087A05 and LC308B01) (Figure 6C). These synergistic effects were largely attributed to a strengthened G_2/M blockade in cell-cycle regulation (Figure 6D and Supplemental Figure 5, C and D) that was a typical consequence of mTOR blockade (37). In line with the mechanism described above, addition of FX1 apparently restored DAPK2 expression and blocked the activation of mTOR signaling triggered by OTX015 in different *KRAS*-mutant NSCLC cell lines
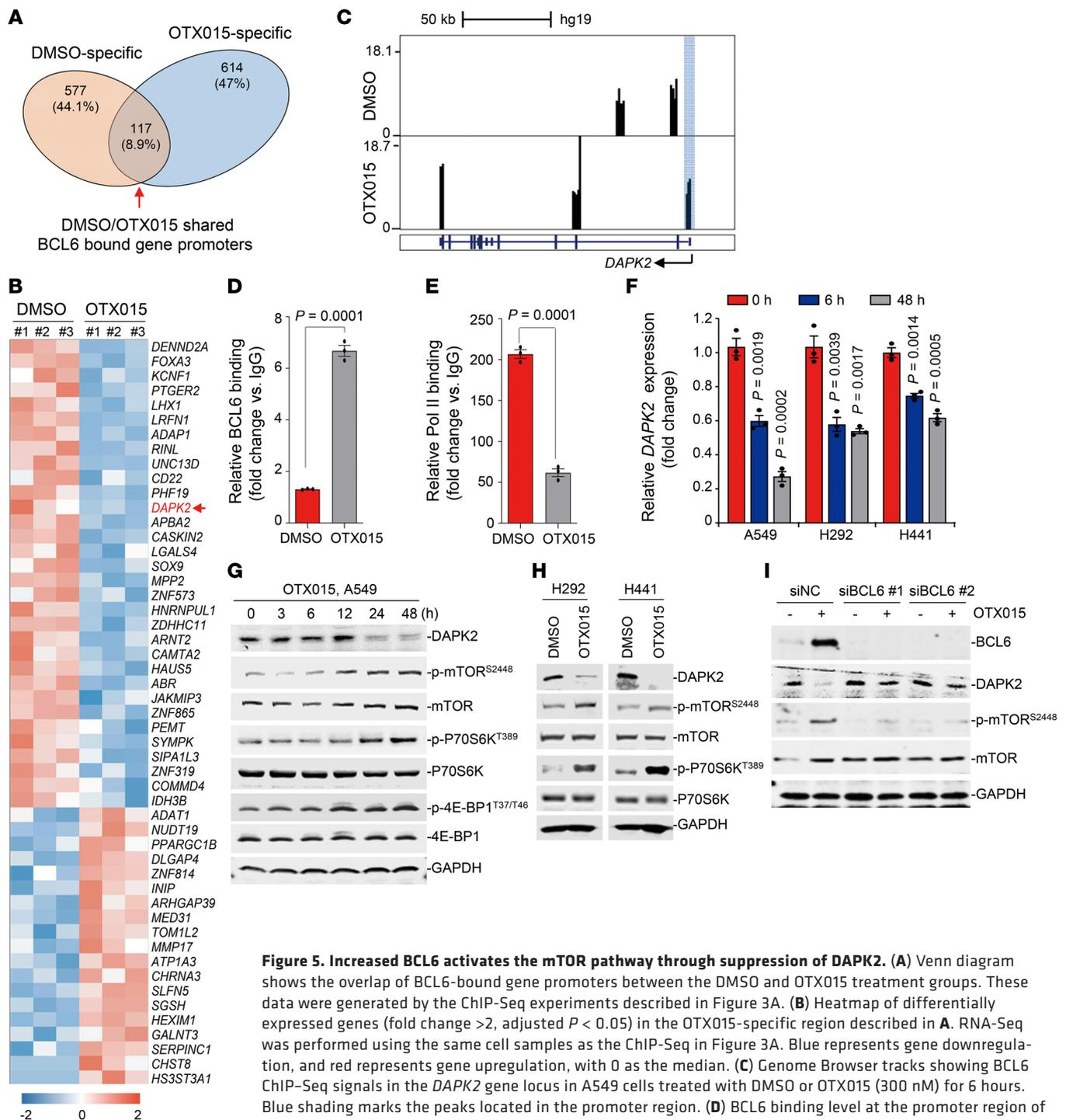
Figure 5. Increased BCL6 activates the mTOR pathway through suppression of DAPK2. (**A**) Venn diagram shows the overlap of BCL6-bound gene promoters between the DMSO and OTX015 treatment groups. These data were generated by the ChIP-Seq experiments described in Figure 3A. (**B**) Heatmap of differentially expressed genes (fold change >2, adjusted $P < 0.05$) in the OTX015-specific region described in **A**. RNA-Seq was performed using the same cell samples as the ChIP-Seq in Figure 3A. Blue represents gene downregulation, and red represents gene upregulation, with 0 as the median. (**C**) Genome Browser tracks showing BCL6 ChIP–Seq signals in the *DAPK2* gene locus in A549 cells treated with DMSO or OTX015 (300 nM) for 6 hours. Blue shading marks the peaks located in the promoter region. (**D**) BCL6 binding level at the promoter region of *DAPK2* examined by ChIP-qPCR assays. (**E**) RNA Pol II–binding level at the promoter region of *DAPK2* examined by ChIP-qPCR assays. Data represent the mean ± SEM of biological triplicates. The P value was determined by comparing the OTX015 treatment group with the control group, using an unpaired, 2-tailed Student's t test. (**F**) Relative *DAPK2* expression at different time points. Cells were treated with 300 nM OTX015, and *DAPK2* mRNA levels were detected by qPCR. Data represent the mean ± SEM of 3 independent experiments. P values were determined by comparing OTX015-treated groups with the untreated group, using an unpaired, 2-tailed Student's t test. (**G**) Effects of OTX015 on the DAPK2/mTOR signaling pathway on A549 cells. A549 cells were treated with OTX015 (300 nM) for the indicated durations. Treated cells were collected and probed with antibodies against DAPK2, p-mTOR (Ser2448), mTOR, p-P70S6K (Thr389), P70S6K, p–4E-BP1 (Thr37/46), 4E-BP1, and GAPDH, respectively. (**H**) Effects of OTX015 on the DAPK2/mTOR signaling pathway in H292 and H441 cells. (**I**) BCL6 knockdown impaired OTX015-mediated DAPK2 suppression and mTOR activation. BCL6 silencing was conducted by RNA interference in A549 cells. Cells were treated with 300 nM OTX015 for 48 hours. Cells lysates were collected and probed with antibodies against BCL6, DAPK2, p-mTOR (Ser3448), mTOR, and GADPH. Immunoblots in **G**, **H**, and **I** were contemporaneous and run in parallel from the same biological replicate, respectively. The immunoblots are representative of at least 3 independent experiments.

(Supplemental Figure 5E), collectively highlighting a core role of BCL6 in BETi-mediated activation of the mTOR pathway.

We next explored the therapeutic efficacy of FX1 and OTX015 cotreatment in vivo by using a patient-derived xenograft (PDX) mouse model with human lung adenocarcinoma tissue harboring a *KRAS*^G12V mutation (LACPDX). Following the schedule described in the clinical trial of OTX015 (ClinicalTrials.gov ID: NCT02259114), we chose a 3-week treatment regimen and found that FX1 significantly enhanced the antitumor effects of OTX015, as indicated by tumor volume (Figure 6E) and tumor weight (Supplemental Figure 6A), without causing significant loss of mouse body weight (Supplemental Figure 6B). More important, the combined therapy did not result in severe systemic toxicity, as serum levels of alanine amino transferase (ALT), aspartame amino transferase (AST), blood urea nitrogen (BUN), and creatinine (CR), along with other biochemical factors, were marginally affected in the treated mice at the end of therapy (Supplemental Table 5). Furthermore, immunoblot analysis of the tumor xenografts showed that protein levels of BCL6 and phosphorylated mTOR (p-mTOR) were remarkably repressed, whereas expression of DAPK2 and p53 (a well-known target gene of BCL6) was reciprocally increased by the combined regimen (Supplemental Figure 6C). These data substantially support the importance of the BCL6/DAPK2/mTOR signaling axis in the resistance of *KRAS*-mutant cancer to BETi in vivo.

On the basis of the synergy of combined BET and BCL6 inhibition on tumor growth in vitro and in vivo, we next investigated the survival benefit of OTX015 plus FX1 in LSL-Kras(G12D) mice, an established genetically engineered mouse model (GEMM) of *KRAS*-mutant lung cancers. To avoid potential toxicity in the GEMM mice, we first tested the safety of the cotreatment of OTX015 and FX1 in normal C57BL/6J mice that shared the same background. Our results showed that the drug pair did not trigger body weight loss in the mice (Supplemental Figure 6D) or any systemic toxicity as determined by the blood cell counts (Supplemental Table 6) and biochemical testing (Supplemental Table 7). Afterward, lung tumors were induced in LSL-Kras(G12D) mice by nasal administration of cre-adenovirus and treated according to the schedule shown in Supplemental Figure 6E. As expected, a substantial therapeutic benefit was achieved with the combined therapy, as indicated by the decrease in tumor size and number (Figure 6, F and G). In comparison with the control, OTX015 monotherapy had a limited effect on mouse survival, whereas addition of FX1 significantly prolonged survival, with an added median survival benefit of 63 days (Figure 6H). Immunohistochemical analysis of tumor tissue additionally demonstrated the involvement of BCL6/mTOR signaling in the response of *KRAS*-mutant lung cancer to BETi (Supplemental Figure 6F). These in vivo data suggest a potent and sustained antitumor activity of combined inhibition of the BET family protein and BCL6.

Activation of an oncogenic allele of Kras is sufficient to initiate tumorigenesis in lung; however, additional tumor suppressor deletion (e.g., *TP53*) leads to significantly advanced adenocarcinoma disease (38). We therefore used the *LSL-Kras*^G12D/+ *Trp53*^fl/fl mouse model to further evaluate the therapeutic efficacy of OTX015 plus FX1 combination therapy. Treatment with the drug pair significantly constrained tumor growth in mice, as shown by micro-CT

images and tumor volume (Figure 6, I and J). Collectively, these findings support the notion that the OTX015 plus FX1 combinative regimen is effective against transformed cells and lung tumor entities harboring a *KRAS* mutation.

mTOR inhibition sensitizes KRAS-mutant NSCLC to BETi. A recent publication (39), together with our results (Figure 5 and Supplemental Figure 6C), prompted us to elucidate the biological function of DAPK2/mTOR signaling in BET resistance. First, we found that p-P70S6K^T389 levels were broadly increased upon OTX015 treatment in cells, suggesting a general effect of OTX015 on mTOR signaling activation, excluding preselection for the p-P70S6K^hi cell population (Supplemental Figure 7A). Next, we found that DAPK2 overexpression inactivated mTOR and significantly sensitized both A549 and H441 cells to BET inhibition (Figure 7, A and B). Finally, genetic silencing of DAPK2 expression prevented the mTOR activation induced by OXT015 (Supplemental Figure 7B). These results support a critical role of the DAPK2/mTOR axis in conferring responsivity of cancer cells to BETi.

Considering that mTOR inhibitors (mTORi) have greater translatability to the clinic than do current BCL6 inhibitors, we further explored the sensitizing effects of the clinically used mTORi rapamycin and ridaforolimus to BETi in vitro and in vivo. Our results showed that mTOR inhibition dramatically enhanced the antigrowth effect of BETi on *KRAS*-mutant NSCLC cells (Figure 7C), in which the CI values were all below 0.7. Besides, we also observed a similar synergistic effect of BETi and mTORi in a long-term colony formation assay (Supplemental Figure 8). Moreover, rapamycin and OTX015 synergized to constrain tumor growth of *KRAS*-mutant LACPDX, as indicated by tumor volume (Figure 7D) and tumor weight (Figure 7E). These data suggest that dual inhibition of BET and mTOR is effective in patients with BETi-resistant *KRAS*-mutant NSCLC.

Discussion

BETi show promising therapeutic effects in clinical trials; however, inherent and acquired resistance is still inevitable, with resistance mechanisms that can be quite complicated in specific tumor contexts, highlighting the need for drug combinations that can potentiate BETi in cancer cells. In this study, we identified a mechanism underlying BETi resistance in *KRAS*-mutant NSCLC, in which BCL6 transcription was markedly promoted as a consequence of BRD3 inhibition. In more detail, we show that BRD3 directly interacted with BCL6 to maintain the BCL6 autoregulatory circuit in unstressed conditions. Intriguingly, such a BRD3-BCL6 complex tends to disassociate from the BCL6 promoter region in response to BETi, consequently leading to increased BCL6 transcription. Moreover, increased expression of BCL6 protein alters its binding mode to negatively regulate the tumor suppressor DAPK2, leading to mTOR signaling activation and conferring resistance to clinical BETi. On the basis of this discovery, we further propose a mechanism-based combinative treatment, in which concurrent inhibition of BET and the BCL6/DAPK2/mTOR axis leads to potent regression of *KRAS*-mutant NSCLC in several tumor mouse models.

BET family members are widely expressed and play a critical role in regulating gene expression by recognizing acetylated histones (3). BRD4 has been considered a transcription activator largely because of its binding to superenhancer regions of several
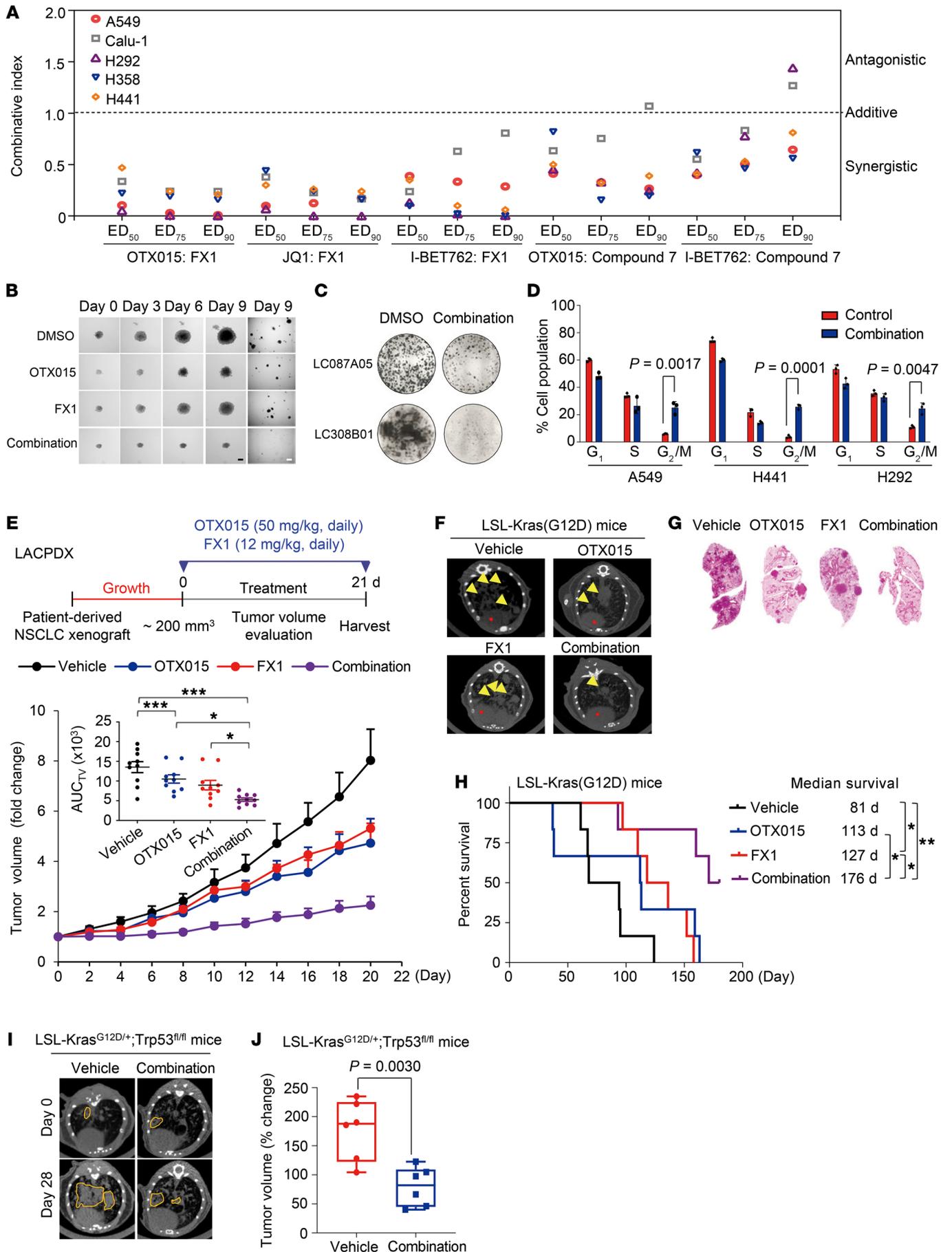
Figure 6. BCL6 inhibitors synergize with BETi in vitro and in vivo. (A) Synergistic interaction between BCL6 inhibitors (FX1 and Compound 7) and BETi (OTX015, JQ1, and I-BET762) in *KRAS*-mutant NSCLC cells. CI values at ED$_{50}$, ED$_{75}$, and ED$_{90}$ were calculated using CalcuSyn software. CI values of less than 1 represent synergism. **(B)** Representative images of 3D colony formation assays of A549 cells in response to the indicated treatments. Scale bars: 0.1 cm (dark) and 1 cm (white). **(C)** Clonogenic assay of primary *KRAS*-mutant NSCLC cells. **(D)** Cell-cycle profiles. Data represent the mean ± SD of biological triplicates. *P* values were determined by unpaired, 2-tailed Student's *t* test, comparing the combination treatment group with the control group. **(E)** Tumor volume (fold change) of patient-derived NSCLC (LACPDX) xenografts in mice (*n* = 10 per group). The mean AUC of tumor volumes (AUC$_{TV}$) on day 21 is shown. Mice were treated according to the schedule in **E**. Data represent the mean ± SEM. *$P < 0.05$ and ***$P < 0.001$, by 1-way ANOVA. **(F)** Representative lung micro-CT images of LSL-Kras(G12D) mice. Yellow arrowheads indicate lung tumors. **(G)** Representative images of H&E-stained unilateral lung lobe tissues after treatment. **(H)** Kaplan-Meier survival analysis of LSL-Kras(G12D) mice (*n* = 6 per group). *$P < 0.05$ and **$P < 0.01$, by log-rank test. **(I)** Representative micro-CT images of the lungs of *LSL-Kras$^{G12D/+}$ Trp53$^{fl/fl}$* genetically engineered mice. Areas marked by yellow dotted lines indicate lung tumors. **(J)** Box plots showing the tumor volumes at the endpoint of the indicated treatments based on micro-CT (*n* = 6 per group). The horizontal lines represent the median, the bottom and top of the boxes represent the 25th and 75th percentiles, respectively, and the vertical bars represent the range of the data. The *P* value in **J** was determined by unpaired, 2-tailed Student's *t* test. All data are shown as the mean ± SEM.

oncogenes (10). In contrast, BRD2 and BRD3 exhibit potential in repressing gene transcription (40, 41). On the basis of our findings, we deem that BRD3 may serve as a tumor suppressor in 2 ways: (a) acting as a BCL6 cofactor to maintain BCL6 autorepression (Figure 4), and (b) protecting BCL6 downstream tumor suppressors (e.g., DAPK2) from BCL6-mediated transrepression (Figure 5). In this study, we found that BRD3 directly interacted with BCL6 protein (Figure 4). The working pattern of BRD3 and BCL6 is similar to that of STAT5 and BCL6, where STAT5 not only mediates the autoregulation of BCL6 (42), but also shares downstream genes with BCL6 (43). The evidence that BCL6 can be inactivated through acetylation by p300 may help to understand the molecular basis of the interaction between BRD3 and BCL6 (44). It is quite possible that BRD3 recognizes the acetyl in BCL6 protein to regulate BCL6 expression, as we found that their interaction was diminished by OTX015 (Supplemental Figure 3D), which selectively inhibits the acetylation-recognizing bromodomain of BET proteins. However, more detailed experiments are required to further elucidate the interaction mode of BCL6 and BRD3.

As a proto-oncoprotein in diffuse large B-cell lymphoma, BCL6 is upregulated in lymphomas and contributes to cancer development (45) as well as drug resistance in leukemia (46–48). However, the biological role of BCL6 in solid tumors has been hard to determine, given its low basal content. Our findings (Figure 1), along with recently published studies (21, 47), support an underestimated function of BCL6 in stressed conditions, in which BCL6 expression can be induced as a consequence of either an increase in its gene transcription or a decrease in its protein degradation. Increased BCL6 expression promotes carcinogenesis and drug resistance by transrepressing a variety of tumor suppressor genes, such as *TP53* (13, 49), *CDKN1A* (50), *PTEN* (51), *DUSP5* (19), and *CASP8* (19). In this study, we found that BCL6

preferentially bound to the *DAPK2* promoter upon BET inhibition (Figure 5, C–F). Suppression of *DAPK2* further led to activation of the mTOR signaling pathway (Figure 5, G–I) to help cells survive BET inhibition (Figure 7, A and B). The critical role of the mTOR pathway in BETi resistance could be consistently supported by the recently published study showing that mTORi synergized BETi in prostate cancer mouse models (39).

BCL6 acts as a transcriptional repressor and engages with a number of corepressors, such as SMRT (52), NCOR (53), and BCOR (54), to an extended groove motif that forms along the BTB dimer interface. Such recruitment relies on the N-terminal BTB domain of BCL6 (55). Inhibition of the BCL6 BTB domain by peptides such as RI-BPI (56) or small molecules such as FX1 (19) and other compounds (57) provided a promising strategy for the treatment of BCL6-driven cancers. Apart from inhibition of the BTB domain, compounds that induced rapid BCL6 protein degradation or targeted a tyrosine residue in the homodimer interface (58) also demonstrated antitumor efficacy. Although BCL6 inhibition has proven to be effective as a monotherapy, our findings, together with those of other studies (21, 47), characterize a critical role of BCL6 in mediating stress tolerance. Therefore, it is of great importance to further evaluate the benefit of BCL6 inhibitors as combinative regimens to conquer BCL6-mediated drug resistance.

Inherent and acquired resistance to BETi often occurs either as a result of increased BET protein expression (7) or a bypass of downstream signaling (9, 10). In our study, we characterized a critical role of the BRD3/BCL6/DAPK2/mTOR axis in conferring BETi resistance and proposed a regimen of dual inhibition of BET and BCL6 to improve the efficacy of BETi in *KRAS*-mutant NSCLC. Importantly, we found that combined therapy targeting BET and BCL6 was effective and well tolerated in 3 different *KRAS*-mutant lung cancer mouse models, including a PDX mouse model, an LSL-Kras(G12D) mouse model, and an *LSL-Kras$^{G12D/+}$ Trp53$^{fl/fl}$* mouse model (Figure 6, E–J). Additionally, combining BETi and BCL6i conferred a remarkable survival benefit in this kind of aggressive and refractory cancer (Figure 6H). Considering that mTORi are more translatable than current preclinical BCL6 inhibitors, we further suggest a more feasible BETi/mTORi combination to circumvent BETi resistance (Figure 7). We believe our findings are of paramount importance, considering that clinical trials of BETi are now being conducted in intractable cancers (ClinicalTrials.gov IDs: NCT02259114, NCT02698176, NCT02630251, and NCT01987362) with limited effectiveness in patients. Additionally, although recent studies revealed that distinguishing BD1 and BD2 of the BET proteins may guide future BET-targeted therapies (59), our findings suggest that development of a BRD4-specific inhibitor may be a pivotal therapeutic option for patients with *KRAS*-mutant NSCLC, as selective inhibition of BRD4 avoids BCL6 upregulation (Figure 4B and Supplemental Figure 3B).

Methods

Detailed methods are provided in the Supplemental Methods.

Cell lines and cell culture. A549, H441, H358, H522, HCT15, DLD1, HCT116, and 293T cells were obtained from the American Type Culture Collection (ATCC). The cell lines Calu-1, H23, H292, H460, LoVo, Capan-2, MDA-Panc-28, SW1990, and MIA PaCa-2 were obtained from
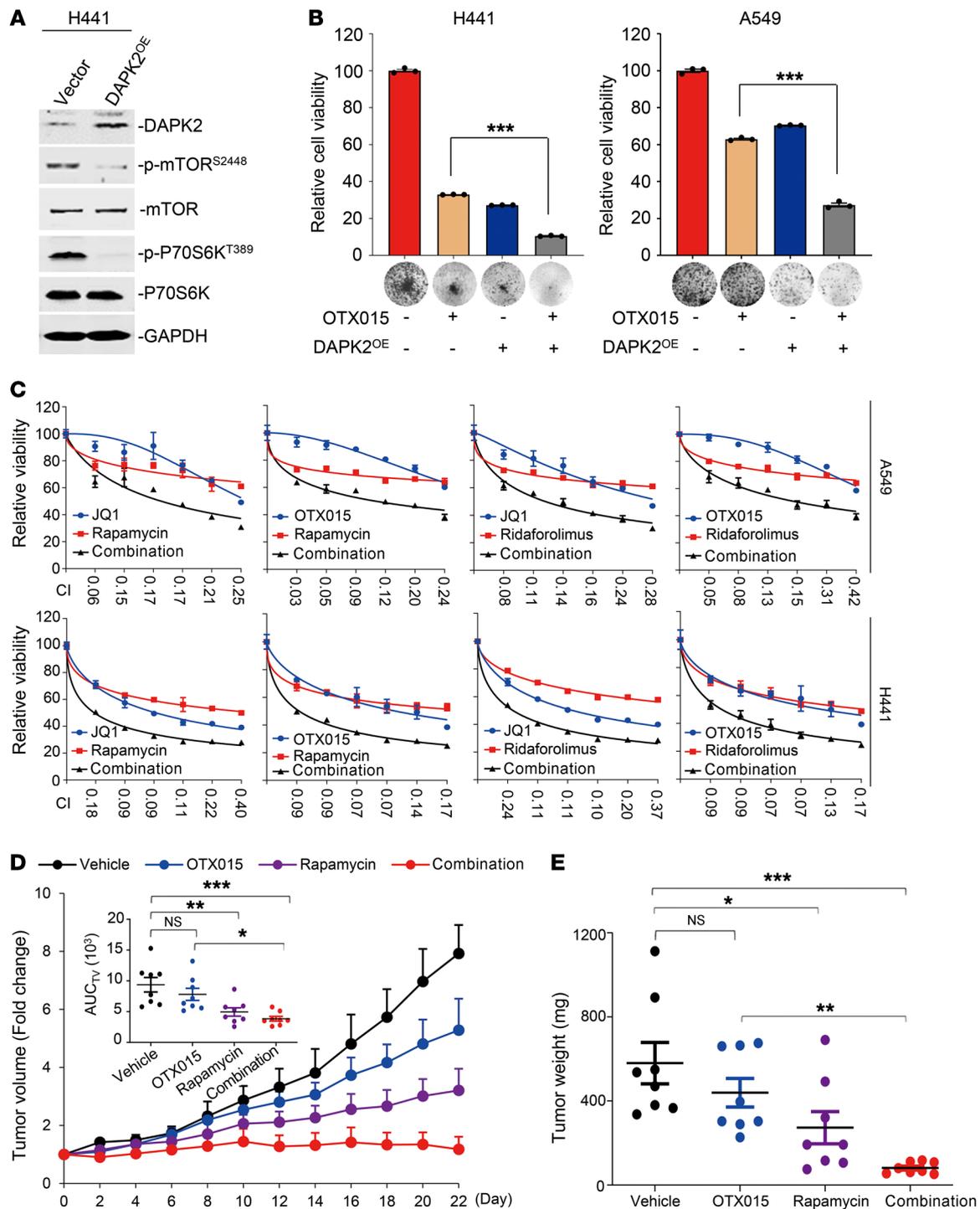
Figure 7. mTOR inhibition sensitizes *KRAS*-mutant NSCLC to BETi. (**A**) DAPK2 overexpression suppressed mTOR and S6K phosphorylation. H441 cells infected with a pCDH-DAPK2 or pCDH control virus were subjected to immunoblot analysis. Immunoblots were contemporaneous and run in parallel from the same biological replicate, respectively. (**B**) Colony formation of H441 and A549 cells with DAPK2 overexpression. Results are representative of 3 independent experiments. Data represent the mean ± SEM of biological triplicates. ***$P < 0.001$, by unpaired, 2-tailed Student's *t* test, comparing the DAPK2^{OE} group with the vector group in the presence of OTX015. (**C**) Synergistic interaction between BETi (OTX015 and JQ1) and mTORi (rapamycin and ridaforolimus) in *KRAS*-mutant NSCLC cells. A549 and H441 cells were treated for 48 hours with various concentrations of the indicated inhibitors. The concentrations of BETi or mTORi were used in a 2-fold dilution series (0.78, 1.56, 3.13, 6.25, 12.5, and 25 μM for individual BETi; 0.78, 1.56, 3.13, 6.25, 12.5, and 25 nM for individual mTORi). Relative cell viability was subsequently measured. Data represent the mean ± SD of biological triplicates. CI values at each concentration were calculated using CalcuSyn software. (**D**) Tumor growth curves of LACPDX (*n* = 8 per group). The mean AUC of tumor volumes on day 23 is shown. Data represent the mean ± SEM. *$P < 0.05$, **$P < 0.01$, and ***$P < 0.001$, by 1-way ANOVA. (**E**) Tumor weights at the end of therapy. Each dot represents a tumor from an individual mouse. Data represent the mean ± SEM. *$P < 0.05$, **$P < 0.01$, and ***$P < 0.001$, by 1-way ANOVA.

the Shanghai Cell Bank of the Chinese Academy of Sciences (Shanghai, China). The HPNE/KRAS[G12V] cells were generated and described previously (60). Briefly, a KRAS[G12V] mutation was introduced into human pancreatic epithelial nestin-expressing (HPNE) cells through a lentiviral delivery system. HPNE/KRAS[G12V] cells were cultured in medium containing 1 volume of M3:Base culture medium (INCELL), 3 volumes of glucose-free DMEM (Thermo Fisher Scientific) supplemented with 10% FBS, 10 ng/mL EGF (R&D Systems), 5.5 nM glucose, and 50 μg/mL gentamycin. Patient-derived lung adenocarcinoma cells LC087A05 and LC308B01 were obtained from 3D Medicines (Shanghai, China) and maintained in DMEM/F12 supplemented with 10% FBS. 293T cells were maintained in DMEM supplemented with 10% FBS. Calu-1 cells were maintained in McCoy's 5A supplemented with 10% FBS, and other cells were maintained in RPMI-1640 medium supplemented with 10% FBS. All cell lines were authenticated by short tandem repeat (STR) analysis and routinely evaluated for mycoplasma contamination.

ChIP-Seq and sequential ChIP assays. The ChIP assays for BCL6 and BRD3 were performed using the SimpleChIP Plus Enzymatic Chromatin Immunoprecipitation kit (agarose beads) (Cell Signaling Technology, 9004) according to the manufacturer's instructions. For ChIP-Seq experiments, A549 cells were treated with 300 nM OTX015 for 6 hours. Cells were cross-linked with 1% formaldehyde for 10 minutes. Consequently, 10× glycine was added and incubated for 5 minutes to terminate the cross-linking. After that, cells were collected and digested with Micrococcal Nuclease (50 Kunitz per sample) for 30 minutes, resulting in an average chromatin fragment size of 150–900 bp. Chromatin from 4×10^6 cells was used for ChIP assays with the following antibodies: anti-BCL6 (Cell Signaling Technology, 14895), anti-BRD3 (Bethyl Laboratories, A302-368A), anti–Pol II (Abcam, ab5408), and normal rabbit IgG (Cell Signaling Technology, 2729). Purified DNA from cells was incubated with the antibody at 4°C overnight followed by washing and reversal of cross-linking. ChIP–Seq libraries were prepared using previously described methods (43), and high-throughput sequencing was performed using an Illumina HiSeq 2000 platform at the Zhongshan Ophthalmic Center of Sun Yat-sen University. Data were analyzed using the following pipeline: ChIP-Seq raw reads were aligned to the human reference genome (GRCh37/hg19) using Bowtie2 (version 2.2.9), and reads mapped to 1 or 2 locations were kept for further analysis. Peak calling was performed by MACS2 (version 2.1.1), with a *P* value threshold of 1×10^{-5}. BigWig files were generated for visualization with the UCSC's Genome Browser (https://genome.ucsc.edu/) or Broad Institute's Integrative Genomics Viewer (IGV) (https://software.broadinstitute.org/software/igv/). The Genomic Regions Enrichment of Annotations Tool (GREAT) (http://great.stanford.edu/public/html/index.php) was used to assign peaks to their potential target genes (a peak gene association was determined if the peak fell into a 2 kb region centered on the transcription start site of the gene). The BCL6 target genes induced by OTX015 were determined independently in each of 2 biological repeat experiments.

Sequential ChIP (ChIP/re-ChIP) was conducted as previously described (61). Briefly, bead eluates from the first immunoprecipitation were incubated with 10 mM DTT at 37°C for 30 minutes, and the resulting samples were diluted 1:50 in dilution buffer (1% Triton X-100, 2 mM EDTA, 150 mM NaCl, and 20 mM Tris-HCl, pH 8.1) followed by immunoprecipitation with the second antibody. DNA pulled down by antibodies or nonspecific IgG was amplified by real-time PCR. The ChIP-qPCR primers are listed in Supplemental Table 8.

Immunoprecipitation. To immunoprecipitate endogenous proteins, whole A549 or H441 cells were lysed in immunoprecipitation buffer (20 mM Tris, pH7.5, 150 mM NaCl, 1% Triton-X 100, protease inhibitor). Cell lysates (1.0–2.0 mg) were precleaned by incubation with protein A/G-agarose beads (Abmart) for 1 hour on a rotator at 4°C. Antibodies against BCL6 (Cell Signaling Technology, 14895, 10 μL), BRD3 (Bethyl Laboratories, A302-368A, 6 μL), and normal rabbit IgG (Cell Signaling Technology, 2729, 1 μL) were added to the precleared lysates and incubated on a rotator at 4°C overnight, respectively. The complex was then immunoprecipitated with protein A/G-agarose beads at 4°C for 1 hour. Beads were washed thrice in immunoprecipitation buffer, resuspended in 50 μL of 2×loading buffer, and boiled at 100°C for 10 minutes. Samples were then analyzed by Western blotting as described in Supplemental Methods.

Reporter assay. Plasmids of pGL4.17 (no. E6721, *Fluc*) and pGL4.74 (no. E6911, *Rluc*) vectors were purchased from Promega. PCR products of the BCL6-binding regions in the *BCL6* gene were purified and subcloned into a modified pGL4.17-basic vector, named P1-Fluc and P2-Fluc, and the empty vector was named P0-Fluc. The amplification primers are listed in Supplemental Table 3. A549 cells were respectively transfected with these plasmids, together with the equivalent *Renilla* luciferase, followed by RNA interference or drug treatment for an additional 48 hours. For coexpression of BCL6 and BRD3, A549 and H292 cells were transfected with a modified luciferase reporter (P1-Fluc), *Renilla* luciferase, pcDNA-BCL6, and/or pcDNA-BRD3. Cells transfected with the equivalent unmodified pGL4.17 and pcDNA3.1 served as controls. Cells were harvested 48 hours after transfection, and luciferase activity was measured using Dual-Luciferase Reporter Assay kits (Promega). Reporter gene activity was determined by normalizing the relevant firefly luciferase to *Renilla* luciferase activity.

Cell viability assays. NSCLC cells were seeded onto 96-well plates at a density of 2000–5000 cells per well and allowed to adhere overnight. Cells were treated with various concentrations of the indicated drugs for 48 hours. Cell viability was determined using the CellTiter 96 Cell Proliferation Assay (Promega) according to the manufacturer's instructions. For the drug synergy analysis, cells were treated with single agents or their fixed-ratio combination for 48 hours. CI values were calculated using CalcuSyn software, version 2 (Biosoft). Combinations with a CI value of less than 1 were considered synergistic, and a CI value of less than 0.7 indicated a strong synergy.

Orthotopic mouse model. A549 cells were digested and resuspended in 50% medium/Matrigel (356234, BD Biosciences) solution. Four-week-old male BALB/cA nude mice were purchased from National Rodent Laboratory Animal Resources (Shanghai, China) and anesthetized with nembutal sodium by intraperitoneal injection. A549 cells were transplanted into the left middle lung at a dosage of $1 \times 10^6/100$ μL per mouse. Fourteen days after transplantation, the mice were orally treated with OTX015 (50 mg/kg/day, daily) for 1 additional week. OTX015 was dissolved in 2% DMSO plus 5% Tween 80 and 30% PEG-400 in double-distilled H_2O (ddH_2O). During the treatment, the mice were randomly sacrificed on day 2 and day 7, and lung cancer tissue was individually isolated using laser capture microdissection technology to determine BCL6 protein levels by immunoblotting.

LACPDX mouse model. Primary *KRAS*-mutant lung adenocarcinoma fragments harboring a KRAS[G12V] mutation were obtained from a patient who underwent surgical resection at Shanghai

Changzheng Hospital (Shanghai, China). The PDX mouse model was established as previously described (25). Fresh patient-derived tumor tissue fragments (~15 mm³) were injected subcutaneously into the flanks of BALB/cA nude mice (National Rodent Laboratory Animal Resources) using a trocar needle. Tumors were measured every other day using electronic calipers, and mouse weight was determined at the same time. Tumor volumes were calculated using the formula: volume = length × width² × 0.52. When tumor volume reached approximately 200 mm³, mice were randomized and treated with vehicle (2% DMSO plus 5% Tween 80 plus 30% PEG-400 in ddH$_2$O), OTX015 (50 mg/kg, orally, dissolved in 2% DMSO plus 5% Tween 80 plus 30% PEG-400 in ddH$_2$O), FX1 (12 mg/kg, intraperitoneally, suspended in 0.5% CMC-Na in sterile water), or OTX015 plus FX1. For the rapamycin experiment, the mice were treated with vehicle, OTX015, rapamycin (3 mg/kg, intraperitoneally, dissolved in 5.2% Tween 80 plus 5.2% PEG-400 plus 89.6% saline), or OTX015 plus rapamycin. On day 21 or 23, the mice were sacrificed, and tumor tissue was excised, weighed, and snap-frozen in liquid nitrogen for Western blot analysis. The blood samples were collected and subjected to biochemical testing (Shanghai ADICON Clinical Laboratories).

LSL-Kras(G12D) mouse model. LSL-Kras(G12D) (B6N.Cg-Kras^{tm4Tyj}/CjDswJ) mice on a C57BL/6J background were purchased from The Jackson Laboratory. C57BL/6J mice were purchased from National Rodent Laboratory Animal Resources. The LSL-Kras(G12D) lung cancer mouse model was generated as previously described by our laboratory (25). Initially, 7-week-old LSL-Kras(G12D) mice were anesthetized with isoflurane via a gas chamber and infected with 5 × 10⁷ infectious particles of Ad-Cre (HanBio) per mouse by intranasal injection. Mice were randomly divided into 4 groups 12 weeks after the operation. Mice were treated with vehicle, OTX015, and/or FX1 daily for 3 weeks. Next, mice were allowed to recover in the untreated condition for an additional week. On day 28, tumors were measured by micro-CT (PerkinElmer) after the final dosing. Meanwhile, 3 mice in each group were randomly sacrificed. Lung tissue was separated for H&E staining and immunohistochemical analysis. The remaining mice (*n* = 6 mice per group) were supported under basic animal care, with no further drug intervention, until their death. Survival rates were calculated by the Kaplan-Meier method. Statistical significance was assessed using log-rank tests.

LSL-Kras$^{G12D/+}$ Trp53$^{fl/fl}$ mouse model. LSL-Kras$^{G12D/+}$ Trp53$^{fl/fl}$ (B6.129-Kras^{tm4Tyj} Trp53^{tm1Brn}/J) mice on a C57BL/6J background were purchased from The Jackson Laboratory. Initially, 8-week-old mice were anesthetized with isoflurane via a gas chamber and infected with 5 × 10⁷ infectious particles of Ad-Cre (HanBio) per mouse by intranasal injection. Mice were randomly divided into 2 groups 8 weeks after the operation. Mice were treated with vehicle and OTX015/FX1 daily for 3 weeks. Next, mice were allowed to recover in the untreated condition for an additional week. On day 28, tumors were measured by micro-CT (PerkinElmer).

Accession numbers. The RNA-Seq and ChIP-Seq data reported here have been deposited in the NCBI's Gene Expression Omnibus (GEO) database (GEO GSE118645 and GSE119863).

Statistics. The data are presented as the mean ± SD unless otherwise stated. Statistical tests were performed using Microsoft Excel and GraphPad Prism, version 5.0 (GraphPad Software). For comparisons of 2 groups, an unpaired, 2-tailed Student's *t* test was used. For comparisons of multiple groups, 1-way ANOVA was used. A log-rank test was performed for survival analysis.

Study approval. All animal treatments were performed according to the *Guide for the Care and Use of Laboratory Animals* (National Academies Press, 2011). All animal procedures were approved by East China Normal University and were performed in accordance with IACUC guidelines. Human lung cancer tissue was obtained from Shanghai Changzheng Hospital (Shanghai, China) with the approval of the ethics committee of Shanghai Changzheng Hospital. Prior written informed consent was obtained from patients.

Author contributions

JG led the project, performed experiments, analyzed data, and wrote the manuscript. YL performed experiments and revised the manuscript. JL, Z. Chen, KL, and JF performed experiments. BZ analyzed the ChIP-Seq and RNA-Seq data. Z. Cai revised the manuscript. LW supervised the quality of the ChIP-Seq and RNA-Seq data and provided experimental support and suggestions. ML provided experimental support and revised the manuscript. XP led the project, analyzed data, and wrote the manuscript.

Acknowledgments

Address correspondence to: Xiufeng Pang, Institute of Biomedical Sciences and School of Life Sciences, East China Normal University, 500 Dongchuan Rd., Shanghai 200241, China. Phone: 86.21.24206942; Email: xfpang@bio.ecnu.edu.cn.

1. Bradner JE, Hnisz D, Young RA. Transcriptional addiction in cancer. *Cell*. 2017;168(4):629–643.
2. Shi J, Vakoc CR. The mechanisms behind the therapeutic activity of BET bromodomain inhibition. *Mol Cell*. 2014;54(5):728–736.
3. Fujisawa T, Filippakopoulos P. Functions of bromodomain-containing proteins and their roles in homeostasis and cancer. *Nat Rev Mol Cell Biol*. 2017;18(4):246–262.
4. Muhar M, et al. SLAM-seq defines direct gene-regulatory functions of the BRD4-MYC axis. *Science*. 2018;360(6390):800–805.
5. Devaiah BN, et al. MYC protein stability is negatively regulated by BRD4. *Proc Natl Acad Sci U S A*. 2020;117(24):13457–13467.
6. Stathis A, Bertoni F. BET proteins as targets for anticancer treatment. *Cancer Discov*. 2018;8(1):24–36.
7. Dai X, et al. Prostate cancer-associated SPOP mutations confer resistance to BET inhibitors through stabilization of BRD4. *Nat Med*. 2017;23(9):1063–1071.
8. Jin X, et al. DUB3 promotes BET inhibitor resistance and cancer progression by deubiquitinating BRD4. *Mol Cell*. 2018;71(4):592–605.e4.
9. Fong CY, et al. BET inhibitor resistance emerges from leukaemia stem cells. *Nature*.

2015;525(7570):538–542.

10. Shu S, et al. Response and resistance to BET bromodomain inhibitors in triple-negative breast cancer. *Nature*. 2016;529(7586):413–417.

11. Cardenas MG, Oswald E, Yu W, Xue F, MacKerell AD, Melnick AM. The expanding role of the BCL6 oncoprotein as a cancer therapeutic target. *Clin Cancer Res*. 2017;23(4):885–893.

12. Margalit O, et al. BCL6 is regulated by p53 through a response element frequently disrupted in B-cell non-Hodgkin lymphoma. *Blood*. 2006;107(4):1599–1607.

13. Phan RT, Dalla-Favera R. The BCL6 proto-oncogene suppresses p53 expression in germinal-centre B cells. *Nature*. 2004;432(7017):635–639.

14. Shvarts A, et al. A senescence rescue screen identifies BCL6 as an inhibitor of anti-proliferative p19(ARF)-p53 signaling. *Genes Dev*. 2002;16(6):681–686.

15. Kurosu T, Fukuda T, Miki T, Miura O. BCL6 overexpression prevents increase in reactive oxygen species and inhibits apoptosis induced by chemotherapeutic reagents in B-cell lymphoma cells. *Oncogene*. 2003;22(29):4459–4468.

16. Pasqualucci L, Migliazza A, Basso K, Houldsworth J, Chaganti RSK, Dalla-Favera R. Mutations of the BCL6 proto-oncogene disrupt its negative autoregulation in diffuse large B-cell lymphoma. *Blood*. 2003;101(8):2914–2923.

17. Walker SR, et al. The transcriptional modulator BCL6 as a molecular target for breast cancer therapy. *Oncogene*. 2015;34(9):1073–1082.

18. Deb D, et al. Combination therapy targeting BCL6 and phospho-STAT3 defeats intratumor heterogeneity in a subset of non-small cell lung cancers. *Cancer Res*. 2017;77(11):3070–3081.

19. Cardenas MG, et al. Rationally designed BCL6 inhibitors target activated B cell diffuse large B cell lymphoma. *J Clin Invest*. 2016;126(9):3351–3362.

20. Kerres N, et al. Chemically induced degradation of the oncogenic transcription factor BCL6. *Cell Rep*. 2017;20(12):2860–2875.

21. Fernando TM, et al. BCL6 evolved to enable stress tolerance in vertebrates and is broadly required by cancer cells to adapt to stress. *Cancer Discov*. 2019;9(5):662–679.

22. Phan RT, Saito M, Kitagawa Y, Means AR, Dalla-Favera R. Genotoxic stress regulates expression of the proto-oncogene Bcl6 in germinal center B cells. *Nat Immunol*. 2007;8(10):1132–1139.

23. Thomas A, Liu SV, Subramaniam DS, Giaccone G. Refining the treatment of NSCLC according to histological and molecular subtypes. *Nat Rev Clin Oncol*. 2015;12(9):511–526.

24. Hu K, et al. Suppression of the SLC7A11/glutathione axis causes synthetic lethality in KRAS-mutant lung adenocarcinoma. *J Clin Invest*. 2020;130(4):1752–1766.

25. Wang J, et al. Suppression of KRas-mutant cancer through the combined inhibition of KRAS with PLK1 and ROCK. *Nat Commun*. 2016;7:11363.

26. Stephen AG, Esposito D, Bagni RK, McCormick F. Dragging ras back in the ring. *Cancer Cell*. 2014;25(3):272–281.

27. Asangani IA, et al. Therapeutic targeting of BET bromodomain proteins in castration-resistant prostate cancer. *Nature*. 2014;510(7504):278–282.

28. Dawson MA, et al. Inhibition of BET recruitment to chromatin as an effective treatment for MLL-fusion leukaemia. *Nature*. 2011;478(7370):529–533.

29. Delmore JE, et al. BET bromodomain inhibition as a therapeutic strategy to target c-Myc. *Cell*. 2011;146(6):904–917.

30. Shimamura T, et al. Efficacy of BET bromodomain inhibition in Kras-mutant non-small cell lung cancer. *Clin Cancer Res*. 2013;19(22):6183–6192.

31. Kikuchi M, et al. Identification of negative regulatory regions within the first exon and intron of the BCL6 gene. *Oncogene*. 2000;19(42):4941–4945.

32. Chiang CM. Phospho-BRD4: transcription plasticity and drug targeting. *Drug Discov Today Technol*. 2016;19:17–22.

33. Britschgi A, et al. DAPK2 is a novel E2F1/KLF6 target gene involved in their proapoptotic function. *Oncogene*. 2008;27(43):5706–5716.

34. Kawai T, et al. Death-associated protein kinase 2 is a new calcium/calmodulin-dependent protein kinase that signals apoptosis through its catalytic activity. *Oncogene*. 1999;18(23):3471–3480.

35. Ber Y, Shiloh R, Gilad Y, Degani N, Bialik S, Kimchi A. DAPK2 is a novel regulator of mTORC1 activity and autophagy. *Cell Death Differ*. 2015;22(3):465–475.

36. Kamada Y, et al. Discovery of a B-cell lymphoma 6 protein-protein interaction inhibitor by a biophysics-driven fragment-based approach. *J Med Chem*. 2017;60(10):4358–4368.

37. Hsieh HJ, et al. Systems biology approach reveals a link between mTORC1 and G2/M DNA damage checkpoint recovery. *Nat Commun*. 2018;9(1):3982.

38. DuPage M, Dooley AL, Jacks T. Conditional mouse lung cancer models using adenoviral or lentiviral delivery of Cre recombinase. *Nat Protoc*. 2009;4(7):1064–1072.

39. Zhang P, et al. Intrinsic BET inhibitor resistance in SPOP-mutated prostate cancer is mediated by BET protein stabilization and AKT-mTORC1 activation. *Nat Med*. 2017;23(9):1055–1062.

40. Denis GV, McComb ME, Faller DV, Sinha A, Romesser PB, Costello CE. Identification of transcription complexes that contain the double bromodomain protein Brd2 and chromatin remodeling machines. *J Proteome Res*. 2006;5(3):502–511.

41. Lamonica JM, et al. Bromodomain protein Brd3 associates with acetylated GATA1 to promote its chromatin occupancy at erythroid target genes. *Proc Natl Acad Sci U S A*. 2011;108(22):E159–E168.

42. Walker SR, Nelson EA, Frank DA. STAT5 represses BCL6 expression by binding to a regulatory region frequently mutated in lymphomas. *Oncogene*. 2007;26(2):224–233.

43. Liu X, et al. Genome-wide analysis identifies Bcl6-controlled regulatory networks during T follicular helper cell differentiation. *Cell Rep*. 2016;14(7):1735–1747.

44. Bereshchenko OR, Gu W, Dalla-Favera R. Acetylation inactivates the transcriptional repressor BCL6. *Nat Genet*. 2002;32(4):606–613.

45. Cattoretti G, et al. Deregulated BCL6 expression recapitulates the pathogenesis of human diffuse large B cell lymphomas in mice. *Cancer Cell*. 2005;7(5):445–455.

46. Béguelin W, et al. EZH2 and BCL6 cooperate to assemble CBX8-BCOR complex to repress bivalent promoters, mediate germinal center formation and lymphomagenesis. *Cancer Cell*. 2016;30(2):197–213.

47. Duy C, et al. BCL6 enables Ph+ acute lymphoblastic leukaemia cells to survive BCR-ABL1 kinase inhibition. *Nature*. 2011;473(7347):384–388.

48. Duan S, et al. FBXO11 targets BCL6 for degradation and is inactivated in diffuse large B-cell lymphomas. *Nature*. 2012;481(7379):90–93.

49. Xu L, et al. BCL6 promotes glioma and serves as a therapeutic target. *Proc Natl Acad Sci U S A*. 2017;114(15):3981–3986.

50. Phan RT, Saito M, Basso K, Niu H, Dalla-Favera R. BCL6 interacts with the transcription factor Miz-1 to suppress the cyclin-dependent kinase inhibitor p21 and cell cycle arrest in germinal center B cells. *Nat Immunol*. 2005;6(10):1054–1060.

51. Wu WR, et al. Amplification-driven BCL6-suppressed cytostasis is mediated by transrepression of FOXO3 and post-translational modifications of FOXO3 in urinary bladder urothelial carcinoma. *Theranostics*. 2020;10(2):707–724.

52. Ahmad KF, et al. Mechanism of SMRT corepressor recruitment by the BCL6 BTB domain. *Mol Cell*. 2003;12(6):1551–1564.

53. Barish GD, et al. The Bcl6-SMRT/NCoR cistrome represses inflammation to attenuate atherosclerosis. *Cell Metab*. 2012;15(4):554–562.

54. Huynh KD, Fischle W, Verdin E, Bardwell VJ. BCoR, a novel corepressor involved in BCL-6 repression. *Genes Dev*. 2000;14(14):1810–1823.

55. Melnick A, et al. Critical residues within the BTB domain of PLZF and Bcl-6 modulate interaction with corepressors. *Mol Cell Biol*. 2002;22(6):1804–1818.

56. Cerchietti LC, et al. A peptomimetic inhibitor of BCL6 with potent antilymphoma effects in vitro and in vivo. *Blood*. 2009;113(15):3397–3405.

57. Paz K, et al. Small-molecule BCL6 inhibitor effectively treats mice with nonsclerodermatous chronic graft-versus-host disease. *Blood*. 2019;133(1):94–99.

58. Teng M, et al. Rationally designed covalent BCL6 inhibitor that targets a tyrosine residue in the homodimer interface. *ACS Med Chem Lett*. 2020;11(6):1269–1273.

59. Gilan O, et al. Selective targeting of BD1 and BD2 of the BET proteins in cancer and immunoinflammation. *Science*. 2020;368(6489):387–394.

60. Chang Z, et al. Cooperativity of oncogenic K-ras and downregulated p16/INK4A in human pancreatic tumorigenesis. *PLoS One*. 2014;9(7):e101452.

61. Wang Y, et al. LSD1 is a subunit of the NuRD complex and targets the metastasis programs in breast cancer. *Cell*. 2009;138(4):660–672.